Available online at www.sciencedirect.com
ScienceDirect
Electrochimica Acta 53 (2008) 4309–4315
ELECTROCHIMICA Acta
www.elsevier.com/locate/electacta

CO tolerance of PdPt/C and PdPtRu/C anodes for PEMFC

Amanda C. Garcia, Valdecir A. Paganin, Edson A. Ticianelli *

Instituto de Química de São Carlos/USP, CP 780, CEP13560-970, São Carlos-SP, Brazil

Received 6 November 2007; received in revised form 17 December 2007; accepted 3 January 2008
Available online 16 January 2008

Abstract

The performance of H_2/O_2 proton exchange membrane fuel cells (PEMFCs) fed with CO-contaminated hydrogen was investigated for anodes with PdPt/C and PdPtRu/C electrocatalysts. The physicochemical properties of the catalysts were characterized by energy dispersive X-ray (EDX) analyses, X-ray diffraction (XRD) and "in situ" X-ray absorption near edge structure (XANES). Experiments were conducted in electrochemical half and single cells by cyclic voltammetry (CV) and I–V polarization measurements, while DEMS was employed to verify the formation of CO_2 at the PEMFC anode outlet. A quite high performance was achieved for the PEMFC fed with H_2 + 100 ppm CO with the PdPt/C and PdPtRu/C anodes containing 0.4 mg metal cm^{-2}, with the cell presenting potential losses below 200 mV at 1 A cm^{-2}, with respect to the system fed with pure H_2. For the PdPt/C catalysts no CO_2 formation was seen at the PEMFC anode outlet, indicating that the CO tolerance is improved due to the existence of more free surface sites for H_2 electrooxidation, probably due to a lower Pd–CO interaction compared to pure Pd or Pt. For PdPtRu/C the CO tolerance may also have a contribution from the bifunctional mechanism, as shown by the presence of CO_2 in the PEMFC anode outlet.

Keywords: PdPt/C catalyst; PdPtRu/C catalyst; PEMFC; CO oxidation; DEMS

1. Introduction

Several investigations focused on the proton exchange membrane fuel cells (PEMFCs) operating with CO-contaminated H_2 had shown that the performance of this system is strongly affected by trace amounts of CO, because CO strongly adsorbs on the Pt anode catalyst surface, causing a drastic decrease of the available active Pt surface sites for the H_2 electrooxidation [1]. Consequently, the electrical current drops to levels that are insufficient for practical applications.

A common approach to diminish this problem consists in the utilization of a second metal in Pt-based anode catalysts, able to form oxygenated species (metal–OH) at potentials lower than pure Pt [2,3]. Following a so-called bifunctional mechanism, these metal–OH species act as a source of oxygen, required for the oxidation of adsorbed CO to CO_2, liberating Pt sites, where the adsorption and oxidation of hydrogen can take place [4]. It has been also proposed that CO tolerance can be achieved by an electronic effect [5,6], which is associated to an energy shift of the Pt 5d electronic states caused by the second element and resulting in a weakening of the Pt–CO interaction. These catalysts have to be stable in the severe environment of the catalyst layer, where a major component is a strong perfluorosulfonic acid. Fuel cell operation may produce changes in the catalyst crystallinity, particle surface composition and the oxidation state of metal, which consequently may decrease the CO tolerance [7].

Among the several possibilities of binary alloys, PtRu has shown the most promising performance for the hydrogen oxidation reaction in the presence of CO [8,9]. However, the low natural abundance of Pt and Ru is a drawback of these catalysts for practical uses and in this sense alternative approaches have been searched, some of them using carbon-supported Pd-rich platinum electrocatalysts with promising results [10,11].

In the present study the CO tolerance on PEMFC anodes containing PdPt/C and PdPtRu/C catalysts prepared by the formic acid reduction method [12] with various Pd:Pt and Ru proportions were examined. The catalyst properties were characterized by energy dispersive X-ray (EDX) analyses, X-ray diffraction (XRD) and "in situ" X-ray absorption near edge structure (XANES). Experiments were conducted in electrochemical half and single cells by cyclic voltammetry (CV) and I–V polarization measurements in some cases coupled with "on line" differential electrochemical mass spectrometry (DEMS). The

* Corresponding author. Tel.: +55 16 3373 9945; fax: +55 16 3373 9952.
E-mail address: edsont@iqsc.usp.br (E.A. Ticianelli).

0013-4686/$ – see front matter © 2008 Elsevier Ltd. All rights reserved.
doi:10.1016/j.electacta.2008.01.006

results of the different techniques allowed a detailed discussion of the CO tolerance mechanism of these materials, including several details not yet available in the literature.

2. Experimental

The 20 wt.% $Pd_xPt_{(100-x)}/C$ ($x = 90$, 80, 70, 60 and 50 atoms%) and $Pd_xPt_yRu_z/C$ ($x = 65$, $y = 25$, $z = 10$ and $x = 25$, $y = 25$, $z = 50$ atoms%) catalysts were prepared by the formic acid reduction method, consisting in the dissolution of the metal precursors (H_2PtCl_6, $PdCl_2$ and $RuCl_3$, Alfa Aesar) in water (~40 mM), which is drop-wise added under stirring to a Vulcan XC-72 (Cabot) carbon 50 mL aqueous dispersion containing 0.5 mol L^{-1} of formic acid at 80 °C [12].

The final compositions of the catalysts were determined by EDX analyses in a scanning electron microscope LEO, 440 SEM–EDX system (Leica-Zeiss, DSM-960) with a microanalyser (Link Analytical QX 2000) and a SiLi detector and using a 20 keV electron beam. The catalysts were also examined by the XRD using a URD-6 Carl Zeiss-Jena diffractometer. The X-ray diffractograms were obtained with an incident wavelength of 1.5406 Å (Kα Cu). The XRD data were used to estimate the Pt lattice parameter and, the average crystallite size using the Scherrer's equation [13].

The materials were also characterized by X-ray absorption spectroscopy (XAS). Measurements were performed at the Pt L_3 absorption edge, with electrodes containing 6 mg cm^{-2} of metal. XAS measurements were made at 0.2 V and 0.5 V vs. RHE (reversible hydrogen electrode), after cycling the working electrode in the range of 0.08–0.5 V vs. RHE. All the experiments were conducted at the XAS beam line in the National Synchrotron Light Source Laboratory (LNLS), Brazil. The data acquisition system for XAS comprised three ionisation detectors (incidence I_0, transmitted I_t and reference I_r). The reference channel was employed primarily for internal calibration of the edge positions by using a pure foil of Pt. The computer program used for analysis of the XAS data was the WinXAS package. Other details were described in the literature [14]. Measurements were made by exploring only the XANES region.

Standard gas diffusion electrodes were prepared with a diffusion layer formed by applying a mixture of carbon powder (Vulcan XC-72R, Cabot) with 15% (w/w) of polytetrafluorethylene (PTFE, TE-306, DuPont) onto both faces of a carbon cloth substrate (PWB-3, Stackpole), using a loading (carbon + PTFE) of 3 mg cm^{-2} per face. To prepare the catalyst layer, a homogeneous suspension formed by 0.1 mL of a Nafion® solution (Aldrich, 5 wt.%), 9.24 mg of Pd_xPt_y/C or $Pd_xPt_yRu_z/C$ (anode) or Pt/C (anode and cathode) electrocatalysts, and ca. 0.05 mL of isopropanol was homogenized in an ultrasonic bath for 10 min and then the solvent was evaporated to dryness. The resulting solid material was dispersed again in isopropanol to produce an ink, which was quantitatively deposited by a brushing procedure in one of the faces of the composite diffusion layer of the electrode [15].

The membrane and electrodes assemblies (MEAs) were prepared by hot-pressing two electrodes (4.62 cm^2, each) on both sides of a pre-treated Nafion® 115 (125 μm) membrane (H^+, DuPont) [15] at 125 °C and 5 MPa, for 2 min. The MEA was placed between high density carbon plates in which serpentine type gas distribution channels were machined.

Cyclic voltammetry and linear sweep CO stripping experiments for the anodes were performed on the gas diffusion electrodes using a potentiostat–galvanostat (Solartron 1285). In these experiments, the anode was used as the working electrode, while the cathode was used as both the counter and the RHE. The cyclic voltammograms were obtained in particular potential range (dependent of the catalyst) at a scan rate of 10 mV s^{-1} and 50 mV s^{-1}. The CO stripping experiments were carried out as follows: after the CO adsorption under potentiostatic control at 100 mV (vs. RHE) for a period of 20 min, the cell was flushed with N_2 for further 40 min to remove the CO excess and finally the anode potential was scanned at 10 mV s^{-1} up to potential sufficient for the stripping of the adsorbed CO.

The polarization experiments in the PEMFC were carried out galvanostatically (Electronic Load HP 6050A) with the cell at 85 °C, using O_2 saturated with water at 90 °C and 0.17 MPa in the cathode, and either pure hydrogen or a mixture of H_2/100 ppm CO saturated with water at 100 °C and 0.2 MPa in the anode. Before the data acquisition, the system was maintained at a cell potential of 0.7 V with pure H_2 for 2 h and at 0.8 V with H_2/100 ppm CO, also for 2 h. The gases were: primary mixture of 100 ppm carbon monoxide in hydrogen balance, nitrogen (99.996%), carbon monoxide (99.5%) and hydrogen or oxygen, all from White Martins.

Measurements of DEMS were performed for understanding the CO oxidation process occurring in the fuel cell anodes [16,17]. The single cell under operating conditions was connected to the mass spectrometer GSD 301 Omnistar from Pfeiffer Vacuum for on line measurements of the CO_2 amount formed at the anode outlet at several cell potentials. The gas analysis system is formed by quadrupole mass (QMS 200, Prisma), having a Faraday cup and a secondary electron multiplier as ion detectors. It has to be pointed that during the system operation, the capillary at the anode outlet was heated at 100 °C to prevent water condensation.

3. Results and discussion

Table 1 presents the results of the EDX analyses. It is seen that the bulk compositions evaluated by EDX present only small discrepancies when compared with the nominal compositions expected from the relative amounts of precursors used in the preparation of the catalysts. Fig. 1 shows the XRD results for these materials. In all cases, the peak distribution indicates the presence of the face-centered cubic structure typical of the palladium or platinum metals. A shift of the diffraction peaks to smaller angles is found in the XRD patterns of PdPt/C and PdPtRu/C catalysts as compared to those of Pd/C, indicating an increase of the lattice constant due to the incorporation of the platinum atoms to the palladium structure. However, the presence of a segregated phase of Pd is evidenced by sharp peaks superimposed to those of alloy features, particularly for $Pd_{60}Pt_{40}/C$.

Table 1
Some physical parameters for the 20 wt.% Pd_xPt_y/C and 20 wt.% $Pd_xPt_yRu_z$/C prepared electrocatalysts, obtained from EDX and XRD analysis

Material	Metal (atom%)			XRD crystallite size (nm)	XRD lattice parameter (nm)
	Pd	Pt	Ru		
Pd/C	100	–	–	12.2	0,3884
$Pd_{90}Pt_{10}$/C	88.4	11.6	–	8.0	0.3879
$Pd_{80}Pt_{20}$/C	79.7	20.3	–	8.0	0.3885
$Pd_{70}Pt_{30}$/C	72.8	27.2	–	8.0	0.3889
$Pd_{60}Pt_{40}$/C	59.9	40.1	–	4.8	0.3892
$Pd_{50}Pt_{50}$/C	54.5	45.5	–	3.2	0.3892
$Pd_{25}Pt_{25}Ru_{50}$/C	31.3	26.1	42.5	3.2	0.3876
$Pd_{65}Pt_{25}Ru_{10}$/C	66.6	24.8	8.5	4.6	0.3879
Pt/C	–	100	–	3.1	0.3919

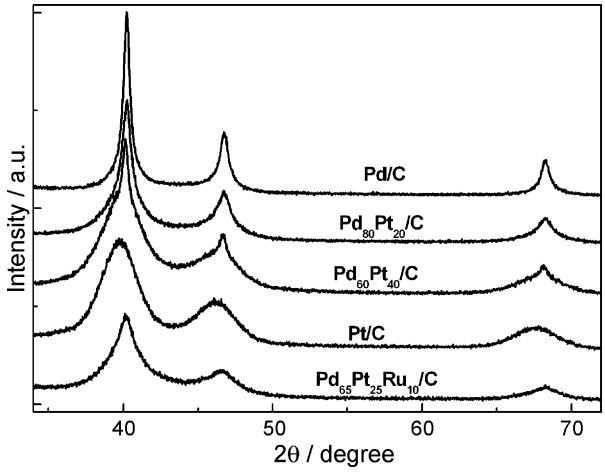

Fig. 1. X-ray diffractograms for PdPt/C and PdPtRu/C catalysts. λ = 1.54056 Å (Kα Cu).

The calculated values of the XRD lattice parameters are included in Table 1. It is seen that for the PdPt/C catalysts, except for $Pd_{90}Pt_{10}$/C, the lattice parameters are higher than the value for pure Pd but smaller than that for pure platinum, and this is consistent to alloy formations. In the case of $Pd_{90}Pt_{10}$/C, specific electronic interactions can be acting causing a lattice reduction with respect to that of pure Pd. For the PdPtRu/C catalysts, the lattice parameters are also smaller than for pure Pd (0.388355 nm, JCPDS card 5–681) and this is due to the interactions with the supports and/or the insertion of Ru (smaller atomic radio than Pd) at the PdPt/C structure.

The metal particle sizes estimated from the XRD data are also included in Table 1. For $Pd_{90}Pt_{10}$/C, $Pd_{80}Pt_{20}$/C and $Pd_{70}Pt_{30}$/C it is seen that the particle sizes are essentially the same (8 nm), while for higher concentration of Pt and for the PdPtRu/C catalysts the sizes are significantly smaller. It has been suggested that Ru promotes the dispersion of the electrocatalyst, because unalloyed amorphous metallic or oxide materials that may reside on or near the surface of the alloy particles help to prevent the particle growth during the deposition [18].

Fig. 2 shows XANES spectra recorded at the Pt L_3 edge for the Pt/C, PdPt/C and PdPtRu/C catalysts, polarized at 200 mV vs. RHE. The X-ray absorption at the Pt L_3 edge corresponds to $2p_{3/2}$–5d electronic transitions and the magnitude of the hump (white line) centered at about 5 eV is directly related to the occupancy of the 5d electronic states. In Fig. 2, a small decrease of the magnitude of the white line is observed in the spectra for PdPt/C and PdPtRu/C compared to that for the Pt/C catalyst. This phenomenon is attributed to a small increase of the Pt 5d band occupancy probably due to a small electron donation of Pd to Pt. Comparing the results for different binary and ternary catalysts it can be verified that the magnitude of the white lines

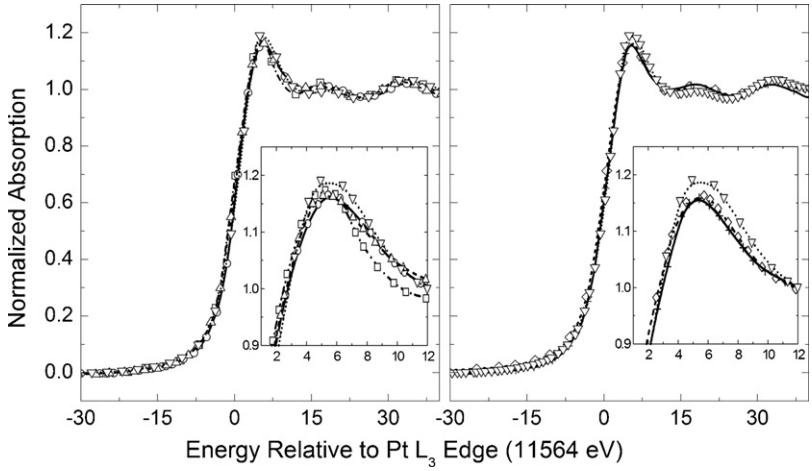

Fig. 2. XANES spectra at the Pt L_3 edge. (□) $Pd_{80}Pt_{20}$/C, (◯) $Pd_{60}Pt_{40}$/C, (△) $Pd_{50}Pt_{50}$/C, (▽) Pt/C, (◇) $Pd_{65}Pt_{25}Ru_{10}$/C, (+) $Pd_{25}Pt_{25}Ru_{50}$/C, at 200 mV vs. RHE. T = 25 °C.

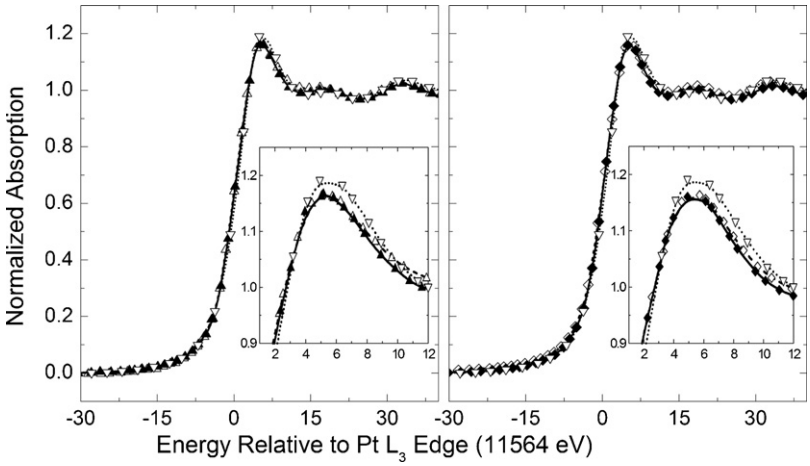

Fig. 3. XANES spectra at the Pt L_3 edge at different potentials vs. RHE. (▽) Pt/C at 200 mV, (△) $Pd_{50}Pt_{50}$/C at 200 mV, (▲) $Pd_{50}Pt_{50}$/C at 500 mV, (◊) $Pd_{65}Pt_{25}Ru_{10}$/C at 200 mV and (♦) $Pd_{65}Pt_{25}Ru_{10}$/C at 500 mV vs. RHE. $T = 25\,^{\circ}C$.

are essentially the same, independent of the Pd concentration or the presence of ruthenium. This in fact confirms that the effect of the Pd and Ru atoms in the electronic properties of Pt is not so pronounced.

Fig. 3 shows XANES spectra at the Pt L_3 edge obtained for (a) $Pd_{50}Pt_{50}$/C and (b) $Pd_{65}Pt_{25}Ru_{10}$/C catalysts at two different electrode potentials. It is seen that the white line magnitude does not change with potential indicating that the eventual presence of Pd hydrides at 200 mV vs. RHE does not play any role on the Pt electronic properties. The present study also shows that the oxide formation on Ru at 500 mV vs. RHE potential, also does not introduce any effect on the electronic properties of Pt. Equivalent observations were made for all alloy catalysts.

In order to improve the understanding of the electrochemical process involved on the electrocatalysts, CV and linear sweep CO stripping experiments were performed. The base cyclic voltammograms are shown in Figs. 4 and 5. In Fig. 4, three voltammetric regions can be distinguished: the hydrogen region between 0.075 V and 0.4 V vs. RHE, followed by the double-layer region up to 0.7 V and oxide formation region above 0.7 V. The upper limit potential was restricted to 0.8 V, since the application of higher values induce irreversible changes in the particle surface composition. Because of the higher stability of Pt and Pd against oxidation and dissolution the most probable cause of these irreversible changes is the migration of a thin Pd-film to the particle surface [19]. The hydrogen region (0.075–0.4 V vs. RHE) on the cyclic voltammogram for the bimetallic catalysts is not so well defined and dependent on the electrodic material [11,20]. In fact the profiles of the hydrogen region are somewhat closer to that of Pd, confirming the formation of the Pd surface film, even for materials not exposed to potentials above 0.8 V vs. RHE and for large Pt contents.

In Fig. 4 it is seen that the currents are smaller for Pd/C and $Pd_{90}Pt_{10}$/C due the higher crystallite sizes (Table 1) in relation to $Pd_{50}Pt_{50}$/C. The double-layer region of the cyclic voltammograms for PdPtRu/C catalysts (Fig. 5) is broader than that for PdPt/C, because of the formation of more oxygenated species involving Ru and also of the larger surface area due to smaller particle sizes [2,3].

Fig. 6 shows the results of the linear sweep CO stripping experiments conducted at 85 °C. The main peak potential moves to more anodic values as the Pd content increases in the catalyst, which is indicative of the stronger CO bonding to Pd. Stronger

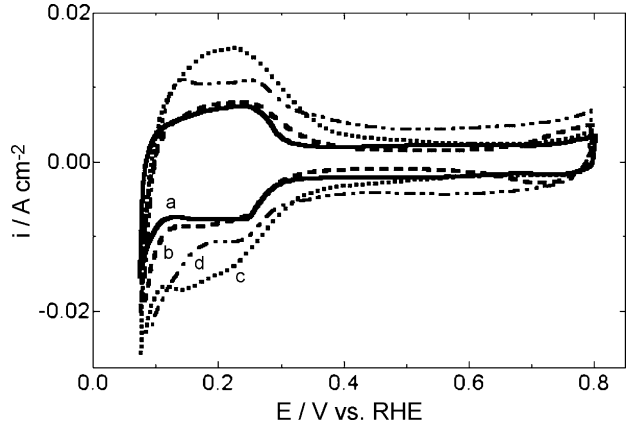

Fig. 4. Cyclic voltammograms for anodes formed by (a) Pd/C, (b) $Pd_{90}Pt_{10}$/C, (c) $Pd_{50}Pt_{50}$/C and (d) Pt/C catalysts. Nafion® 115 membrane; $T = 27 \pm 2\,^{\circ}C$; $v = 50\,mV\,s^{-1}$.

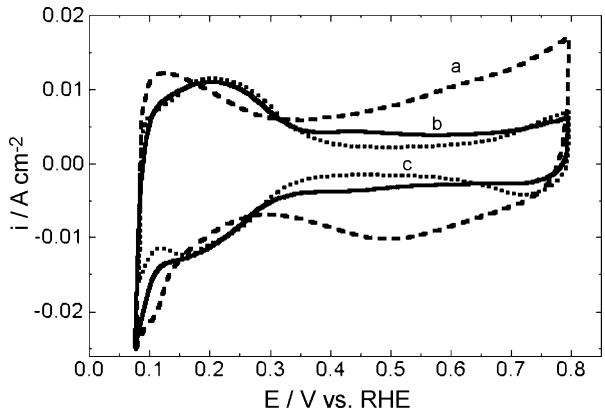

Fig. 5. Cyclic voltammograms for anodes formed by (a) $Pd_{25}Pt_{25}Ru_{50}$/C, (b) $Pd_{65}Pt_{25}Ru_{10}$/C and (c) $Pd_{70}Pt_{30}$/C catalysts. Nafion® 115 membrane; $T = 27 \pm 2\,^{\circ}C$; $v = 50\,mV\,s^{-1}$.

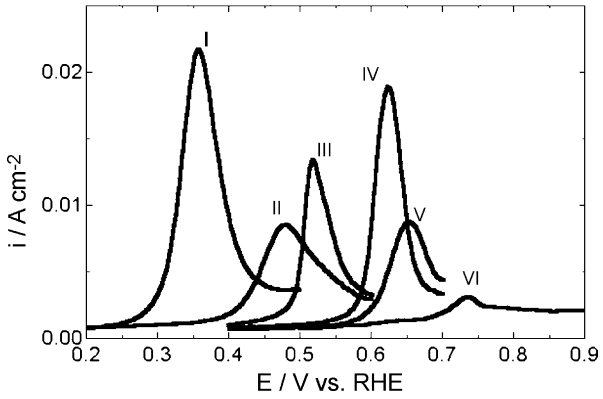

Fig. 6. CO stripping scans for anodes formed by: (i) $Pd_{25}Pt_{25}Ru_{50}$/C, (ii) $Pd_{65}Pt_{25}Ru_{10}$/C, (iii) Pt/C, (iv) $Pd_{60}Pt_{40}$/C, (v) $Pd_{90}Pt_{10}$/C and (vi) Pd/C. Electrosorption at 100 mV (vs. RHE). Nafion® 115 membrane; $T = 85\,^{\circ}C$; $v = 10\,mV\,s^{-1}$.

anion adsorption on Pd may also play a role in diminishing the oxidation reaction rate [21].

For carbon-supported Pt, the limited particle size favours the formation of linearly bonded species, with the CO molecule occupying atop sites [22]. Bridge-bonded CO is the predominant species on palladium [23]. While CO from PtPd may originate from both Pt and Pd atoms, the oxidation involves only a single uniform peak. A synergistic effect is thus evident; the peak is not simply an addition of fractional contributions of Pt and Pd sites. Electronic modification of the CO adsorption characteristics on the two metals, due to bimetallic particle formation, is clearly supported by the results in Fig. 6. However, in Fig. 6 it is seen that the CO adsorption characteristics in the PdPt/C catalysts located in the intermediate position between Pt/C and Pd/C but are closer to that of Pd even for large Pt contents, and having the desorption charges increasing with the increase of the Pt content. Since the cyclic voltammetries evidenced the presence of a Pd surface layer in all cases, these results suggest a strong modification of the Pd–CO bond characteristics, compared to bare Pd.

For the PdPtRu/C catalysts the main contribution to the shift of the CO stripping peak to lower potentials is the presence of Ru, which is more easily electro-oxidized than pure Pt and Pd, and forms $Ru–OH_{ads}$ species at lower potentials, helping to oxidize the adsorbed CO through the bifunctional mechanism.

Fig. 7a shows potential vs. current density plots for H_2/O_2 PEMFC single cells fed with pure hydrogen with Pt/C cathodes and with Pd/C, PdPt/C, PdPtRu/C and Pt/C anodes. The results with pure hydrogen show that the performance of the system with Pd/C drops considerably when compared to Pt/C. On the other hand, the results for PdPt/C and PdPtRu/C electrodes show practically the same result as for Pt/C even for a Pt content as low as 10 atoms%, in agreement to the data reported in literature [11,24]. It is also seen that in these last cases the cells present the typical performance profiles, with the polarization losses dominated by the oxygen reduction activation overpotentials at low current densities, which is coupled with linear and non-linear ohmic losses at moderate and high current densities, respectively [25]. A very large change of the HOR kinetics on the Pd skin layer, compared to bulk Pd, is suggested by these

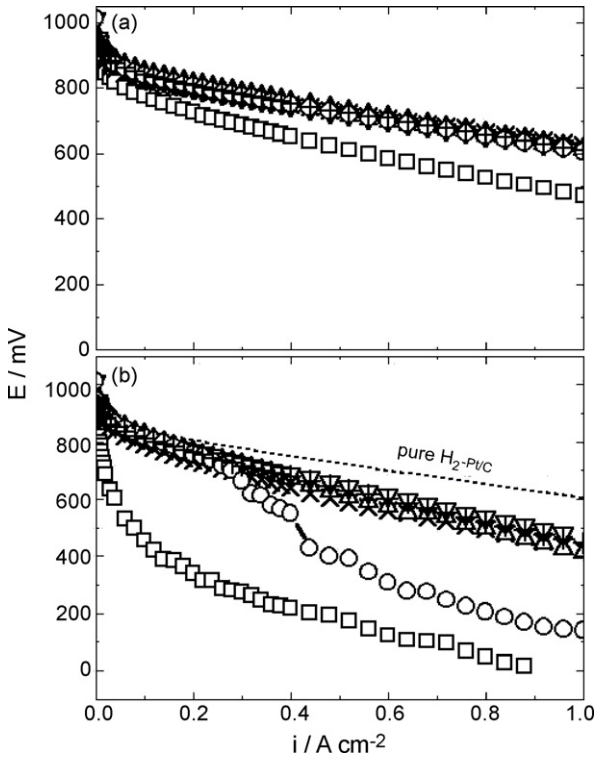

Fig. 7. Cell potential vs. current densities for PEMFCs with (□) Pd/C, (○) Pt/C, (×) $Pd_{90}Pt_{10}$/C, (△) $Pd_{80}Pt_{20}$/C, (▽) $Pd_{60}Pt_{40}$/C and (+) $Pd_{25}Pt_{25}Ru_{50}$/C anodes (0.4 mg metal cm^{-2}). (a) Anodes fed with pure H_2 and (b) anodes fed with H_2 + 100 ppm CO, both saturated with water at 100 °C and 0.2 MPa. Cathodes with Pt/C (0.4 mg Pt cm^{-2}) fed with O_2 saturated with water at 90 °C and 0.17 MPa. Nafion® 115 and cell at 85 °C.

results, which is most probably related to a change of the Pd–H bond strength.

Steady-state polarization curves for PEMFC anodes fed with hydrogen containing 100 ppm CO, are presented in Fig. 7b. As expected, results show that the performance of the systems drops considerably when the CO-containing H_2 is introduced to the anode, particularly for Pd/C and Pt/C. On the other hand, the results for the PdPt/C and PdPtRu/C electrodes show that the performance with H_2 + 100 ppm CO is much better than for the pure noble metal catalysts.

In Fig. 8a the overpotentials of the hydrogen electrode ($\eta_{H_2/CO}$) caused by the presence of CO are plotted as a function of the current density in the single cell. The overpotentials were calculated as $\eta_{H_2/CO} = E_{H_2} - E_{H_2/CO}$, where E_{H_2} and $E_{H_2/CO}$ are the cell potentials in the absence and in the presence of CO, respectively. For the PdPt/C catalysts the overpotential of the anode presents small differences for the electrodes with different Pd to Pt ratios, with the best result seen for $Pd_{60}Pt_{40}$/C. For materials containing Ru the best result is for $Pd_{25}Pt_{25}Ru_{50}$/C.

The production of CO_2 in the anode of the single cells was monitored by on line DEMS measurements for the system working at 85 °C and the results are presented in Fig. 8b in terms of the CO_2 ($m/z = 44$) ion current gain plotted as a function of the hydrogen electrode overpotential ($\eta_{H_2/CO}$). The ion current gain is defined as $\Delta I/I_0$, where ΔI is the difference of the currents measured with the cell fed with H_2/CO (I) and H_2 (I_0). For sys-

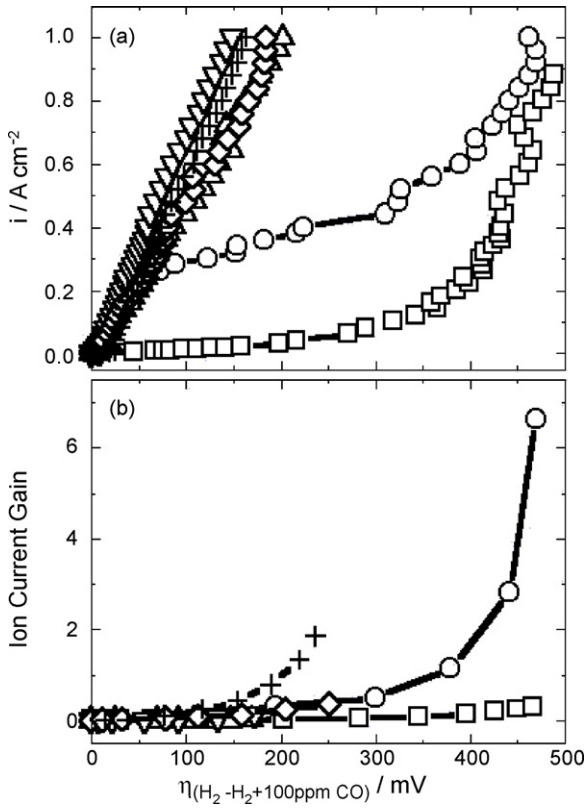

Fig. 8. (a) Overpotential vs. current density and (b) production of CO_2 (ion current gain) vs. cell overpotential obtained by DEMS for single cells fed H_2 + 100 ppm CO for (□) Pd/C, (○) Pt/C, (△) $Pd_{80}Pt_{20}$/C, (▽) $Pd_{60}Pt_{40}$/C, (◊) $Pd_{65}Pt_{25}Ru_{10}$/C and (+) $Pd_{25}Pt_{25}Ru_{50}$/C. The overpotentials were calculated as $\eta_{H_2/CO} = E_{H_2} - E_{H_2/CO}$, where E_{H_2} and $E_{H_2/CO}$ are the cell potentials in the absence and in the presence of CO, respectively.

tems with the Pt/C and PdPtRu/C anode catalysts, gains of the current related at $m/z = 44$ are observed, while no change of the base-line are seen for PEMFCs with the PdPt/C anodes from the beginning to the end of the potential variations.

Several observations can be employed to discuss the improved CO tolerance of the PdPt/C catalysts:

i) the presence of a Pd layer on the surface of the PdPt/C particles is suggested, either by the cyclic voltammetry or the CO stripping experiments. This layer may present distinct hydrogen and CO adsorption properties, as compared to bulk Pd, as suggested by the CO stripping and the fuel cell experiments;
ii) although not so pronounced, there is an increase of occupation of the Pt 5d band in the PdPt/C catalysts compared to Pt/C, as shown by the XANES results. This effect would imply an opposite effect with respect to the Pd atoms;
iii) for the PdPt/C catalysts there is no CO_2 formation even for situations where the HOR current generation is above 1 A cm^{-2}, in contrast to Pt/C for which, before CO_2 formation, the current does not go more than 0.3–0.4 A cm^{-2}; in any case, this observation for Pt/C allows to conclude that even for this material there are vacancies on the CO adsorbed layer enough to generate considerably high HOR currents.

Based on the above facts one would conclude that the main characteristic of the PdPt/C catalysts is to present a reduced degree of coverage of CO in the Pd surface layer, enough for the anode to provide currents of the order of 1 A cm^{-2}, without too much potential losses. This effect is surely related to an electronic effect of Pt on Pd and vice-versa, because this is done in a range of potentials where no CO_2 formation was detected in the anode outlet. In the case of the catalysts with Ru, the DEMS experiments clearly demonstrated CO_2 formation under the same conditions, thus evidencing a contribution of the bifunctional mechanism in the generation of free surface sites.

4. Conclusions

The polarization curves showed higher tolerance to CO of the PdPt/C and PdPtRu/C catalysts, as compared to Pd/C and Pt/C. A quite high performance was achieved for the PEMFC fed with H_2 + 100 ppm CO with anodes containing 0.4 mg metal cm^{-2}, with the cell presenting overpotentials always below 200 mV at 1 A cm^{-2}, with respect to the system fed with pure H_2. XANES results indicated that electronic interactions of the Pd and Pt atoms are very small, while the presence of a Pd layer on the surface of the PdPt/C particles is suggested either by the cyclic voltammetry and the CO stripping experiments. This layer may present distinct hydrogen and CO adsorption properties, as compared to bulk Pd. No CO_2 formation was detected in the anode outlet when the PdPt/C catalysts are considered. So, the improved performance was assigned to the fact that the PdPt/C catalysts present smaller CO coverage with the HOR occurring in the vacancies of such layer. For PdPtRu/C the CO tolerance also presents a contribution of the bifunctional mechanism as shown by the presence of CO_2 in the anode outlet.

Acknowledgements

The authors thank the financial support of the Fundação de Amparo a Pesquisa do Estado de São Paulo (FAPESP—Proc. 04/10788-5), Conselho Nacional de Desenvolvimento Científico e Tecnológico (CNPq) and FINEP, Brazil. The authors also thank the National Synchrotron Light Source Laboratory (LNLS) and Carlos Bento for the XAS and EDX experiments, respectively.

References

[1] T.J. Schmidt, M. Noeske, H.A. Gasteiger, R.J. Behm, P. Britz, W. Brijoux, H. Bönnemann, Langmuir 13 (1997) 2591.
[2] W.F. Lin, T. Iwasita, W. Vielstich, J. Phys. Chem. B 103 (1999) 3250.
[3] A. Pozio, L. Giorgi, E. Antolini, E. Passalacqua, Electrochim. Acta 46 (2000) 555.
[4] S.J. Lee, S. Mukerjee, E.A. Ticianelli, L. McBreen, Electrochim. Acta 44 (1999) 3283.
[5] E. Christoffersen, P. Liu, A. Ruban, H.L. Skriver, J.K. Norskov, J. Catal. 199 (2001) 123.
[6] L. Giorgi, A. Pozio, C. Bracchini, R. Giorgi, S. Turtu, J. Appl. Electrochem. 31 (2001) 325.
[7] F.A. Uribe, J.A. Valerio, F.H. Garzon, T.A. Zawodzinski, Electrochem. Solid-State Lett. 7 (2004) A376.

[8] A. Kabbabi, R. Faure, R. Durand, B. Beden, F. Hahn, J.M. Leger, C. Lamy, J. Electroanal. Chem. 444 (1998) 41.
[9] H.A. Gasteiger, N.M. Markovic, P.N. Ross Jr., J. Phys. Chem. B 99 (1995) 8290.
[10] P. Stonehart, Int. J. Hydrogen Energy 9 (1984) 921.
[11] D.C. Papageorgopoulos, M. Keijzer, J.B.J. Veldhuis, F.A. de Bruijn, J. Electrochem. Soc. 149 (2002) A1400.
[12] A.L.N. Pinheiro, A. Oliveira-Neto, E.C. de Souza, J. Perez, V.A. Paganin, E.A. Ticianelli, E.R. Gonzalez, J. New Mater. Electrochem. Syst. 6 (2003) 1.
[13] A.R. West, Solid State Chemistry and its Applications, Wiley, Chichester, 1984, pp. 734.
[14] G.A. Camara, M.J. Giz, V.A. Paganin, E.A. Ticianelli, J. Electroanal. Chem. 537 (2002) 21.
[15] V.A. Paganin, E.A. Ticianelli, E.R. Gonzalez, J. Appl. Electrochem. 26 (1996) 297.
[16] L.G.S. Pereira, M.E. Pereira, E.A. Ticianelli, Quimica Nova 30 (2007) 1644.
[17] S. Wasmus, J.-T. Wang, R.F. Savinell, J. Electrochem. Soc. 142 (1995) 3825.
[18] M.P. Hogarth, T.R. Ralph, Platinum Met. Rev. 46 (2002) 146.
[19] G.A. Attard, A. Bannister, J. Electroanal. Chem. 300 (1991) 467.
[20] M. Lukaszewski, A. Czerwinski, Electrochem. Acta 51 (2006) 4728.
[21] B. Alvarez, V. Climent, A. Rodes, J.M. Feliu, J. Electroanal. Chem. 497 (2001) 125.
[22] D.C. Papageorgopoulos, F.A. de Bruijn, J. Electrochem. Soc. 149 (2002) A140.
[23] K. Kunimatsu, J. Phys. Chem. 88 (1984) 2195.
[24] Y.-H. Cho, B. Choi, Y.-H. Cho, H.-S. Park, Y.-E. Sung, Electrochem. Commun. 9 (2007) 378.
[25] D.R. de Sena, E.A. Ticianelli, V.A. Paganin, E.R. Gonzalez, J. Electroanal. Chem. 477 (1999) 164.